The first-order anisotropy (A_1, ϕ_1) has been used to determine whether the magnetosphere corotates with the planet and to observe field-aligned particle flow. The former quantity can be measured most easily if the scan plane is perpendicular to $\overline{B}$. In that case

$$A_1/A_o \simeq \left[\frac{1}{A_o} \frac{\partial A_o}{\partial v} - \frac{2}{v} \right] \overline{\phi}_1 \cdot \overline{v}_c + \rho_g \overline{\phi}_1 \cdot \frac{\nabla A_o}{A_o} \times \frac{\overline{B}}{B} \tag{5.11}$$

where v is the particle velocity, $\overline{v}_c$ is the corotation or $\overline{E} \times \overline{B}$ velocity, $\overline{\phi}_1$ is a unit vector in the direction of the first-order anisotropy, ρ_g is the gyroradius, and $\overline{B}$ the magnetic field. A number of terms have been dropped which are normally small in a dipole field [Birmingham and Northrop, 1979]. The first term in Equation (5.11) is the Compton–Getting effect, which permits a determination of the local plasma velocity, provided the gradient effect given by the second term can be evaluated.

In principle, a more accurate determination of the local plasma velocity is possible from the angular distribution of low energy particles, because the anisotropies are larger and the gyroradii (gradient effects) are smaller. These data have shown (Chap. 4) that the plasma velocity is generally parallel to the corotation direction. However, the magnitude of the velocity was derived mostly from high-energy data (Fig. 5.11) because the low energy ion composition, hence, ion velocity, could be determined accurately at only a few places (Chaps. 3 and 4). The middle magnetosphere moves in the general direction of corotation much of the time, but significant departures in magnitude (and sometimes direction) occur beyond 20 R_J (see also McNutt, Belcher, and Bridge [1981]). First-order anisotropies in energetic electron distributions are negligibly small because, at equal energies, electrons have a much higher speed and smaller gyroradii than protons. The question of corotation is further discussed in Chapters 3, 4, and 11.

Angular distributions of protons in the middle magnetosphere have also been observed when the magnetic field made a small angle relative to the scan plane. In that case, the first-order anisotropy contains an additional term that is proportional to particle flow along the magnetic field. This has been interpreted in terms of an actual transport of protons away from the equator [McDonald, Schardt, and Trainor, 1979; Northrop, Birmingham, and Schardt, 1979] and a short residence time [Northrop, 1979]. However, these observations were made during periods when the magnetic field was swept back and had a large component parallel to the $\Omega \times \overline{r}$ corotation velocity, and, therefore, at least a fraction of the field-aligned velocity does not represent an actual transport of particles. The surprising discovery of large fluxes of energetic oxygen and sulfur ions [Krimigis et al., 1979a] in the middle magnetosphere raises the possibility that the combined response to protons plus heavy ions may account for much of the first-order anisotropies and that any actual transport of particles is below previous estimates.

Proton pitch-angle distributions, as reflected by the second-order anisotropy, are pancake near the equator. Such a distribution would be a consequence of the magnetic-pumping model suggested by Goertz [1978]. The distribution is often sufficiently flat to be near or just beyond the onset of the mirror instability [Northrop and Schardt, 1980] which redistributes pitch angles, as is required by the magnetic-pumping model.

Energetic-electron pitch angle distributions near the equator are almost isotropic between 25 and 45 R_J. The A_2/A_o term is only a few percent, giving a slightly pancake shape. Between 20 and 25 R_J, however, the electron distributions are strongly field aligned (that is, dumbbell) as would be expected from the recirculation model

(Chap. 10). In this model, electrons diffuse at a high latitude (small pitch angles) from the inner magnetosphere to field lines that extend into the middle magnetosphere.

A major effort has gone into defining the dynamic processes in the middle magnetosphere and the degree to which the three adiabatic invariants [Northrop, 1963] are conserved. One approach is to use Liouville's theorem and adiabatic theory to correlate particle distribution functions, and, hence, particle fluxes at different points along a field line. This permits calculating the intensity along a field line by using the equatorial distribution function and the magnetic field configuration. If stable trapping conditions exist in the middle magnetosphere, the particle energy is constant along a field line and pitch-angle scattering can be ignored. Under these conditions, the flux at a pitch angle δ is the same as the flux at a pitch angle δ_2 at a different point along the same field line, provided the pitch angles are related by

$$\sin \delta = \sqrt{B/B_2} \sin \delta_2 \tag{5.12}$$

Usually one relates the flux to the equatorial values; in this case, δ_2 and B_2 are equatorial pitch-angles and field magnitudes. Consequently, the intensity of an isotropic distribution is invariant along a field line, and a pancake distribution of the form $C(1 + \sin^2 \delta_o)$ at the equator will transform into $C(1 + B_o/B \sin^2 \delta)$ at a point where the field strength has increased from B_o to B. Calculations using a local field model developed for this purpose have been performed for 0.5- and 1.3-MeV electrons, and for 0.5- and 1.9-MeV protons in the region from 20 to 30 R_J [Schardt and Birmingham, 1979]. The electron flux modulation observed during the Pioneer 10-inbound pass was closely predicted by this picture; however, the predicted proton flux modulation is much smaller than observed. Observed fluxes about 8 R_J below the magnetic equator are only 1/5 to 1/3 as large as predicted by this model.

Three different factors may cause or contribute to this discrepancy.

1. A flux change by a factor of 3 to 5 with System III longitude could produce the effect; however, there is no evidence to support such a large longitudinal dependence.
2. The proton intensity depends on local time (see section entitled Predawn magnetosphere). The magnetic field lines through an observation point 8 R_J below the magnetic equator cross the equator at an earlier local time. The field model used to fit the Pioneer 10 data in this region [Schardt and Birmingham, 1979] gives a difference of only 10° or 40 min. in local time; however, the available field data do not permit a unique solution. Based on the change in flux with local time (Pioneer 10 inbound vs. outbound), a difference of 2 to 3 hr would probably be required to account for the observations.
3. Some of the assumptions about stable trapping may be invalid. Extensive electromagnetic and plasma wave activity were observed in the middle magnetosphere (Chap. 8); however, specific waves that could account for the energetic particle observations have not been identified.

At times, proton spectra changed rapidly owing to preferential acceleration between 1 and 3 MeV. Figure 5.12 shows successive spectra taken 15 min. apart at about 37.5 R_J when the spacecraft was well below the magnetic equator. The 0345 spectrum is a typical exponential in momentum. Thirty minutes later, a distinct peak appeared near 2 MeV which then relaxed to a plateau between 1 and 3 MeV. This plateau was observable for about two hours. Essentially no change in the slope of the spectrum was

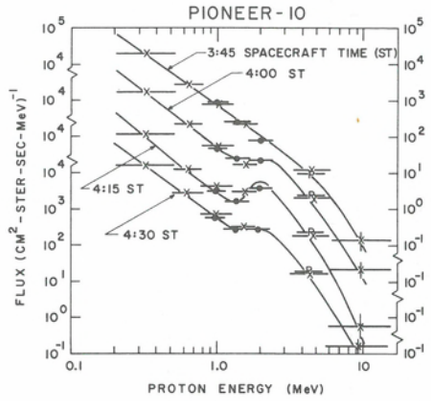

Fig. 5.12. Proton spectra (15-min. average) observed by Pioneer 10-in between 37.3 and 37.8 R_J on December 2, 1973. Note the enhanced flux between 1.5 and 3 MeV at 4:15 spacecraft time. The data were taken with the GSFC/UNH instrument. The solid circles and P's represent LET-I data and the crosses LET-II data (see Table 5.1).

seen at lower or higher energies, and only a small change was observed in the total flux. A probable explanation is resonant proton acceleration over a limited energy range by a plasma wave. Unfortunately, the absence of simultaneous wave measurements prevented the identification of the specific mechanism.

Large, rapid changes in proton flux provide additional strong evidence for particle acceleration. These events were first described by Simpson et al. [1975; see also Simpson and McKibben, 1976]. An outstanding example of such a flux change was a tenfold increase in the 0.5- to 5-MeV proton flux that occurred in 10 min. at 32 R_J when the spacecraft was about 7 R_J below the magnetic equator [Schardt, McDonald, and Trainor, 1978]. Before and after the event, the flux was characteristic of the low level normally encountered at this distance from the magnetic equator. The relative proton fluxes and their pitch-angle distributions are shown in Figure 5.13. Owing to an inclination between the magnetic field and the scan plane, fluxes at small pitch angles could not be sampled. At 1255, the small proton flux was relatively isotropic with a small field-aligned component indicating a flow towards Jupiter. A considerably higher flux was observed at 1302 but with little change in angular distribution. At peak intensity (1305), a strong field-aligned injection was observed. Because of the rapid flux increase and a 5-minute half-bounce period, most of the protons had not yet mirrored. The magnetic field signature showed that a current sheet passed across the spacecraft at the same time. Alpha particles and/or heavier ions were accelerated as well as protons, but their flux peaked at a slightly different time.

Because the proton spectrum was unchanged by this event, it is quite possible that this type of process is responsible for the normally observed proton population in the middle magnetosphere. Numerous such acceleration events of various magnitudes may occur with the greatest number in the plasma sheet; however, the spacecraft would only see a time average because it is normally not at the exact site of the acceleration process. The superposition of numerous events could give rise to the rms fluctuations in the counting rate shown in Figure 5.7. These fluctuations have been defined in terms of the difference between counting rates N_i and N_{i+1} taken 1.6 min. apart:

$$< \Delta N >_{\text{rms}} = \left(\frac{1}{10} \sum_{i=1}^{10} (N_i - N_{i+1})^2 \right)^{1/2} \tag{5.13a}$$

$$< \frac{\Delta N}{N} >_{\text{rms}} = \left(\frac{1}{10} \sum_{i=1}^{10} \left(\frac{N_i - N_{i+1}}{1/2(N_i + N_{i+1})} \right)^2 \right)^{1/2} \tag{5.13b}$$

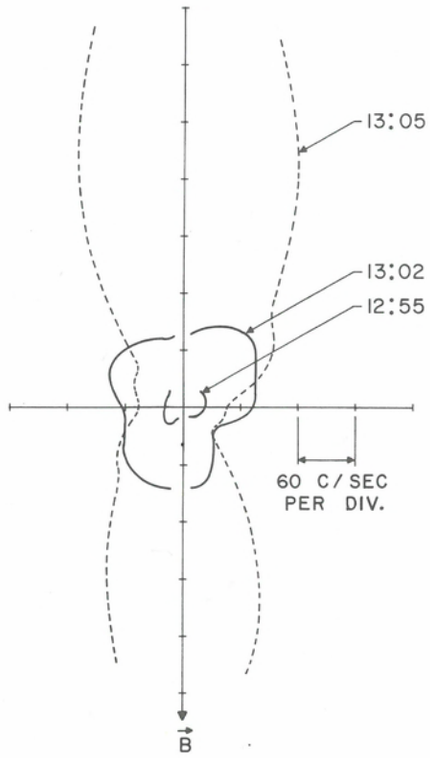

Fig. 5.13. Pitch angle distribution (in the corotating frame) of 1.15- to 2.15-Mev protons at 32 R_J in subsolar hemisphere. The data were taken with LET-II of the GSFC/UNH experiment on Pioneer 10.

Because counting statistics also produce random fluctuations, the observed rms values are plotted only when the probability is greater than 95% (χ^2 test) that the effect is not statistical.

As can be seen from Figure 5.7, the largest fluctuations ($<\Delta N>_{\text{rms}}$) occur close to the plasma sheet of the middle magnetosphere, as would be expected if the equatorial plasma sheet is the region of greatest activity. In contrast, the percentage proton fluctuations are largest in regions where the flux drops most rapidly, perhaps because the proton flux along a field line does not follow simple trapping theory.

Fluctuations in proton fluxes at different energies are highly correlated with less than 6 min. time delay due to a differential drift. In contrast, cross correlation between fluctuations in electron and proton fluxes is small. A lack of cross correlation would be expected if the fluctuations are due to wave particle interactions because protons and electrons interact with an entirely different part of the spectrum. In contrast, radial gradients in the proton and electron fluxes are in the same direction, and strong cross-correlation would be expected if the fluctuations were caused by bulk motion, that is, expansion and contraction of the magnetosphere.

These observations lead to the following conclusions: (a) the observed fluctuations are primarily due to actual changes in the population of a flux tube rather than to motion of drift shells with different particle intensities; (b) any specific flux enhancement is dissipated in a few minutes; (c) most, if not all, the flux changes are produced by processes occurring near the equator; and (d) the same process affects a wide range of particle energies, but discriminates between protons and electrons.

Outer magnetosphere

Pioneer observations of electron and proton fluxes in the subsolar outer magnetosphere (45 R_J to the magnetopause) are shown in Figures 5.6, 5.7, and 5.8. Because the magnetopause position responds sensitively to solar wind pressure [Smith, Fillius, and Wolfe, 1978], the outer magnetosphere is repeatedly being compressed and then allowed to expand. This continuous pumping should contribute substantially to the irregular magnetic field configuration and changes in energetic particle fluxes. That fluxes increased when the magnetosphere was compressed is suggested by the higher fluxes observed when the magnetopause crossed the spacecraft in response to compression (change from magnetosphere to magnetosheath) than when the magnetosphere expanded. This effect is particularly noticeable for the large compression observed by Pioneer 10 inbound near 55 R_J (Fig. 5.6).

Particle spectra in the outer magnetosphere are similar to those in the middle magnetosphere. Electron spectra are somewhat harder, as reflected in a value for H (Equation 5.8) between 15 and 35, rather than 2 to 5, as in the middle magnetosphere. Owing to a relative increase in <1-MeV protons, the proton spectra become a power law, $E^{-\gamma}$, with γ between 3 and 4. An acceleration event of protons near 2 MeV has been observed at 73 R_J and resembled the one illustrated in Figure 5.12.

First-order anisotropies dominate angular distributions in the outer magnetosphere. For electrons, field-aligned streaming was observed (Sentman and Van Allen, 1976) with Pioneer 10 at 64 and 52 R_J. The latter coincided with a known compression of the magnetosphere. First-order anisotropies of protons are generally in agreement with corotation out to about 65 R_J, although they fall frequently below the rigid-corotation value (Fig. 5.11). This was particularly evident during the Pioneer 10 inbound pass. The first-order anisotropies did not reflect corotation in either magnitude or direction beyond 75 R_J [McDonald, Schardt, and Trainor, 1979]. This variability is not surprising, because changes in magnetopause position could produce high local plasma velocities throughout much of the outer magnetosphere. Second-order anisotropies in the outer magnetosphere are variable and may be either pancake or dumbbell.

A regular 9 hr 55 min. modulation of the high-energy electron flux (>5 MeV) was found in the outer magnetosphere (Figs. 5.6 and 5.8). It was originally suggested that the equatorial plasma sheet may extend to the magnetopause and produce the modulation by the same mechanism as in the middle magnetosphere. Such an interpretation is not borne out by the magnetic field configuration [Smith et al., 1976]. Throughout the outer magnetosphere, the field is quite irregular; it generally has a southward component, and clear-cut plasma sheet crossings are not observed. A study of the phase of this modulation is also inconsistent with a plasma sheet modulation and will be discussed in the section on Modulation [McKibben and Simpson, 1974; Fillius and Knickerbocker, 1979].

Although lower energy ions (<1 MeV/nuc., Chap. 4) already show an enhancement of oxygen and sulfur, energetic ions (~ 7 MeV/nuc) in the outer magnetosphere (Fig. 5.4) have the composition of solar cosmic rays rather than the enhanced oxygen and sulfur abundance found in the inner magnetosphere. Their intensity was, however, significantly higher than in interplanetary space; thus, acceleration has to be invoked to raise their energy above the instrumental threshold. It may be concluded that energetic particles in the outer Jovian magnetosphere are subject to dynamic processes in this region of high-β plasma. The primary driving mechanism is presumably due to changes in solar wind pressure and plasma diffusing out from the inner magnetosphere. Magnetospheric asymmetries may provide a modulation mechanism for high-energy electrons. It should be noted that Kivelson [1976] has identified a turbulent boundary layer

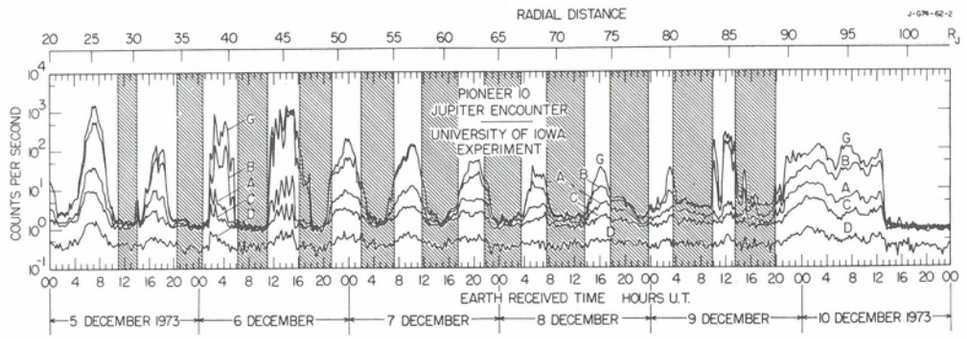

Fig. 5.14. Count rates of the University of Iowa experiment observed during Pioneer 10-out. The shaded areas correspond to times when Pioneer 10 was on open field lines [from Goertz et al., 1976b].

that may be identical with the outer subsolar magnetosphere. Such a boundary layer may be formed by outflowing magnetospheric plasma [Chap. 11; Dessler, 1979]. As yet, this layer has not been theoretically discussed in any detail for the Jovian magnetosphere but should prove a very challenging concept for theoreticians.

5.4. Predawn magnetosphere

Observations

In the antisolar hemisphere, the magnetospheric plasma is no longer compressed by the solar wind and expands into a relatively thin plasma sheet which has been identified by its magnetic signature to distances beyond 200 R_J [Behannon, Burlaga and Ness, 1981]. The particle fluxes are heavily modulated (Figs. 5.14 and 5.15), and the modulation of electrons and protons is in phase. Intercomparison with magnetic field data shows that flux maxima occur at crossings or approaches to the plasma sheet. A close anticorrelation is always found between the magnetic field strength and both the electron [Van Allen, 1979] and proton fluxes [Walker, Kivelson, and Schardt, 1978; Goertz, Schardt, and Van Allen, 1979]. Because particles above 200 keV are responsible for only a minor fraction of the field decrease, we believe that energetic particles constitute the high-energy tail of the thermal plasma in the sheet.

Whereas Pioneer 10-out encountered only one particle maximum per rotation (Fig. 5.14), the lower-latitude Voyager spacecraft saw two maxima at least out to 80 R_J and Voyager 2 frequently to beyond 150 R_J (Fig. 5.15). The following picture emerges: the predawn magnetosphere contains a current sheet in which energetic particles are trapped. The sheet is inclined with respect to the rotational axis and thus moves up and down relative to the equatorial plane, passing a low latitude spacecraft twice per rotation and approaching a high latitude spacecraft once per rotation. Near the central plane of the current sheet the magnetic field lines are closed, but field lines at higher latitudes are presumably open and cannot trap particles (Chap. 1) [Goertz et al., 1976b; Connerncy, Acuña, and Ness, 1981]. In the region of open field lines, the flux drops to interplanetary levels and the plasma density (Chaps. 3 and 4) reaches extremely low values. This effect is illustrated in Figure 5.14, where shading indicates when Pioneer 10 was on open field lines. The large difference between the subsolar and antisolar magnetosphere beyond 20 R_J is quite obvious if one compares Figures 5.6, 5.7, and the left side of Figure 5.8 with Figures 5.14 and 5.15. The plasma sheet modulation of

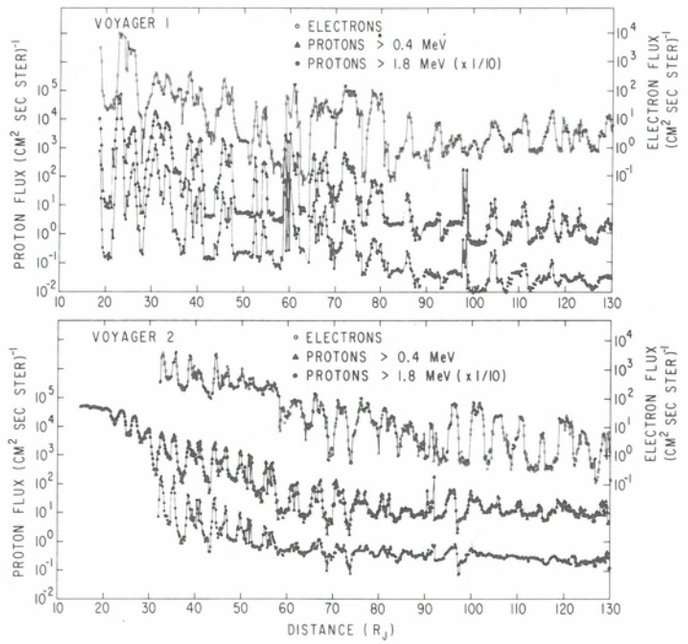

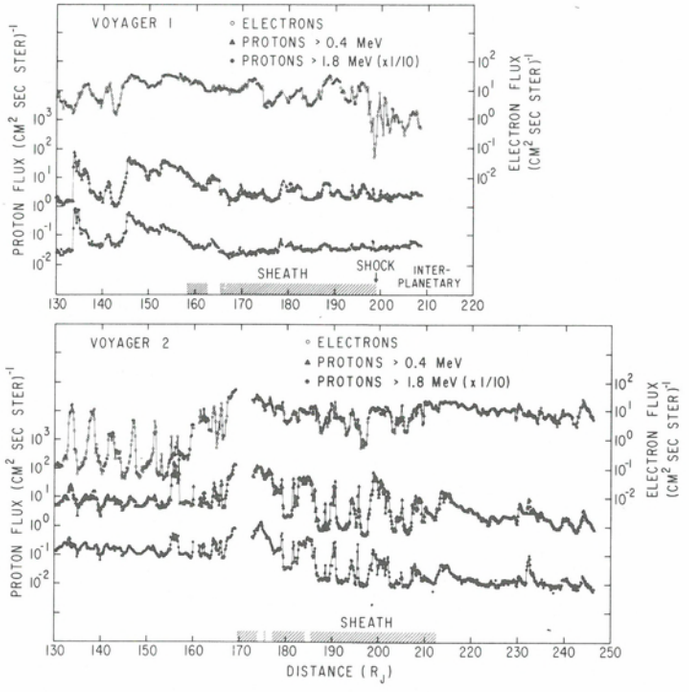

Fig. 5.15. Electron (2.6–5.1 MeV) and proton fluxes (16-min. average) observed by the CIT/GSFC experiment on Voyagers 1 and 2 towards $-115°$ and $-137°$, respectively, from the Jupiter–Sun line. Electron and >1.8-MeV proton fluxes above 10^3 cm^{-2} s^{-1} st^{-1} are uncertain because of large correction and are plotted only to show relative trends [from Schardt, McDonald, and Trainor, 1981].

particle fluxes is generally less pronounced at local times 0800 to 1200 and extends to only 45 R_J. Plasma sheet configurations that are consistent with the observed modulation will be discussed in the next section.

An intercomparison of absolute flux levels between inbound and outbound passes shows that energetic-particle fluxes in the predawn plasma sheet are generally $\leq 10\%$ of equivalent fluxes at the same distance in the subsolar hemisphere. Unfortunately, time variability of the trapped energetic-particle flux and problems associated with intercomparing data from different instruments preclude a determination of the local time at which minimum flux is reached. However, indications are that the flux does not change much between local times of 0200 and 0600 but increases rapidly between 0600 and 1100. This observation confirms predictions of the magnetic pumping process (Chap. 10) provided the major azimuthal change in the field configuration occurs between 0600 and 1200.

Strong flux gradients make it difficult to determine the plasma convection velocity from the first-order anisotropy of energetic protons (see discussion under middle magnetosphere). The low energy data (Chap. 4) show that the convection velocity is in the direction of corotation and the higher energies indicate [Carbary et al., 1981; Schardt et al., 1981] that the magnitude is often consistent with rigid corotation, but more detailed analysis is required to confirm the preliminary results. Based on observations in the subsolar hemisphere, it is to be expected that the plasma convection velocity is substantially lower than corotation, but no free expansion into the tail takes place (Chaps. 3 and 4).

First-order anisotropies from Pioneer 10-out showed, starting at $\sim 15\ R_J$, a consistent radial outflow of energetic protons [Sentman, Van Allen, and Goertz, 1975]. This indicates that the trapping lifetime should be relatively short. In contrast, the second-order anisotropy in the plasma-sheet region is either zero (isotropic) or slightly pancake, which is an indication of a long trapping lifetime. No such radial outflow was observed during the Voyager passes [Carbary et al., 1981], thus indicating that trapping lifetimes are normally long.

Near flux maxima, the proton and electron spectra were nominally the same as in the subsolar hemisphere. A typical proton spectrum at 64.9 R_J under quiescent conditions is shown in Figure 5.16*c*. Consistent with the prediction of open field lines at flux minima, the proton spectra and fluxes in the tail lobe resemble those of interplanetary protons (Fig. 5.16*a*).

As in the terrestrial magnetotail, disturbed conditions occur also in the Jovian predawn magnetosphere. Periods of enhanced and irregular proton flux can be seen in Figure 5.15*a* for Voyager 1 near 60 and 100 R_J. Under these conditions, the spectral shape depends on pitch angle (Figs. 5.16*b* and *d*). Protons with small pitch angles (LET-B) have a softer spectrum than locally mirroring protons. During the 59 R_J event, a large local intensity gradient must have existed (2.6 times per R_J toward center of plasma sheet) to account for the intensity ratio (5–10) between two detectors that pointed perpendicular to the magnetic field. The event near 100 R_J is an example of protons streaming away from Jupiter along magnetic field lines. Several short bursts, lasting about 10 min. each, were observed during which the flux of protons coming from Jupiter was greatly enhanced (up to 40:1) over the flux at $\sim 90°$ pitch angles. As can be seen from Figure 5.16*d*, the two spectra were quite different.

Three different types of activity have been observed near the plasma sheet [Schardt, McDonald, and Trainor, 1981]:

1. General flux increase with a hardening of the spectrum and moderate anisotropies were observed at 45 and 59 R_J.

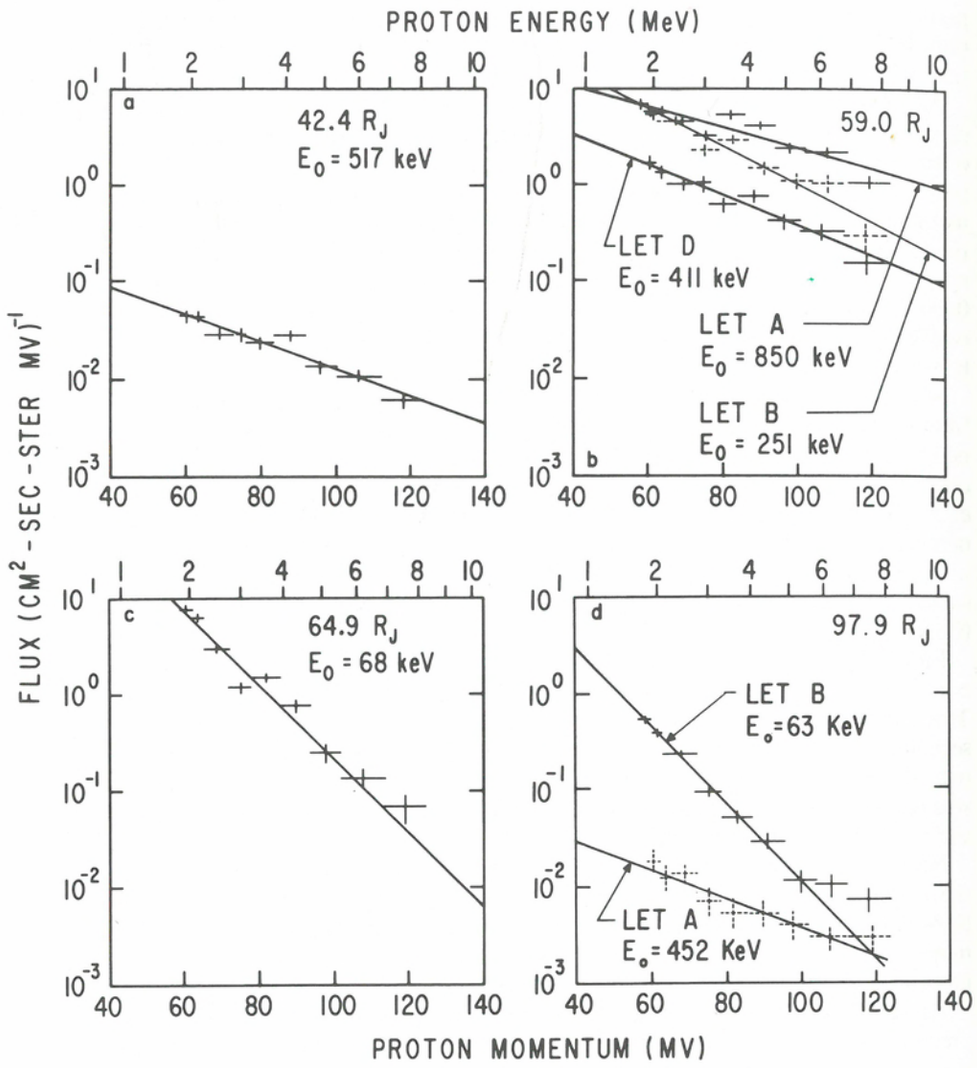

Fig. 5.16. Proton momentum spectra (64-min. average) observed during the outbound pass of Voyager 1 with the CIT/GSFC LET detector. The spectrum at 42.4 R_J was taken in the tail lobe, the 59.0 R_J spectra represents an acceleration event, the 64.9 R_J spectrum gives a typical quiescent plasma sheet population and the 97.9 R_J spectra were observed during field-aligned streaming. LET-B pointed towards Jupiter within about 20° of the magnetic field direction, and LETs *A* and *D* pointed approximately perpendicular to the field direction [from Schardt, McDonald, and Trainor, 1981].

2. Outward flow along an ordered field configuration was observed at 98 and 133 R_J.
3. Outward flow in an irregular field configuration was observed in the boundary layer inside the magnetopause at 155 R_J with Voyager 2. This was also observed at lower energies [Krimigis et al., 1980] and can be explained in terms of a rapid convective motion of the thermal plasma.

At a distance of 10 to 20 R_J inside the magnetopause, the strong periodic modulation of the energetic-particle flux ceases; the electron flux increases to its prior value in the plasma sheet and remains that high even in the sheath region outside the magnetosphere (Figs. 5.14 and 5.15). Intensity changes are smaller and less regular. This region appears to be a boundary layer, which has also been identified by the enhanced population of thermal electrons [Gurnett et al., 1980]. The properties of this boundary layer resemble in many respects the outer magnetosphere in the subsolar direction. The region just inside the magnetopause as observed with Voyager 2 has also been interpreted in terms of a planetary wind [Krimigis et al., 1979b] because the first order anisotropy indicates a convection velocity away from Jupiter (Chap. 4) and the magnetopause does not constitute a sharp barrier to the particles.

Rotational modulation

A rotational modulation of the energetic particle flux can be accounted for in principle by three models. As so often occurs in physics, reality requires different models in different regions of the magnetosphere.

The clock model [McKibben and Simpson, 1974] asserts that the modulation is due to a global 10-hr modulation of the magnetosphere, either its size, its trapped particle content or its energy. The observed time variation of particle flux j is taken to be a real-time derivative

$$\text{clock modulation:} \quad \frac{dj}{dt} = \frac{\partial j}{\partial t} \tag{5.14a}$$

The magnetic anomaly model [Dessler and Hill, 1975] asserts that the 10-hr modulation is due to a preferred longitude (related to a surface magnetic anomaly) sweeping past the spacecraft. The observed time variation is due to the rotation of a longitudinal asymmetry

$$\text{magnetic anomaly:} \quad \frac{dj}{dt} = \Omega \frac{\partial j}{\partial \lambda} \tag{5.14b}$$

where Ω is Jupiter's angular velocity and λ the longitude of the spacecraft.

The disc model [Van Allen et al., 1974a] asserts that the modulation is due to a rotational modulation of the spacecraft's magnetic latitude ψ_m. Such a modulation is due to the fact that the magnetic dipole is tilted with respect to the rotational axis. In this case

$$\text{disc modulation:} \quad \frac{dj}{dt} = \Omega \frac{\partial j}{\partial \psi_m} \frac{\partial \psi_m}{\partial \lambda} \tag{5.14c}$$

Note that this model can be formulated in different versions depending on whether ψ_m is measured from the surface of minimum magnetic field or the magnetic dipole equator.

In its pure form the clock model postulates that the modulation phase and period are independent of the observer's zenographic latitude or local time. The magnetic

anomaly model postulates that the period is independent of latitude and local time but that the phase is dependent on local time. In contrast to these, the disc model predicts a dependence of both phase and period on the observer's location. A spacecraft in the zenographic rotational equator should see a 5-hr modulation if the plausible assumption is made that j is symmetric about $\psi_m = 0$. In analogy to the Earth's magnetotail [Ness, 1965], an additional mechanism may have to be considered in the predawn magnetotail. This is a rocking motion of the neutral sheet about the Sun–Jupiter line in response to solar-wind interaction with the dipole [Behannon, Burlaga, and Ness, 1981; see also Chap. 1]. Because of the large distances at Jupiter, however, propagation delays become quite significant, and it is not yet clear what neutral sheet configuration this process would produce.

Figure 5.17 shows the phase of the Pioneer 10 electron (6- to 30-MeV) modulation relative to the expected position in the basic disc model, where the disc is represented by the dipole equator. As can be seen from this figure, this model holds in the middle magnetosphere out to about 35 R_J. It should be noted that a 180° phase shift relative to the disc model would have been introduced at closest approach if the modulation followed either the clock or anomaly model. The reason is that Pioneer 10 crossed the equator at periapsis and, therefore, the inbound and outbound passes were on opposite sides of the dipole equator.

In the outer magnetosphere (inbound pass ~60 to 90 R_J) the phase is advanced by ~110°; outbound it lags by 220 to 260° beyond 90 R_J (Fig. 5.17). Thus, the phase shift is one period. The 10-hr modulation of Jovian electrons in the plasma sheath surrounding the magnetosphere and in interplanetary space is also in phase [Chenette, Conlon, and Simpson, 1974]; thus, it appears that the electron flux varies simultaneously in these regions. The Voyager 2 data taken above, rather than below, the magnetic equator (Fig. 5.8) are in phase (synodic period) with Pioneer observations below the equator [Schardt, McDonald, and Trainor, 1981]. The clock model applies in these regions because the disc model requires a 180° phase shift between Pioneer 10-in and Voyager 2-in data, and the magnetic anomaly model would not predict the observed 360° phase shift between the Pioneer 10 inbound and outbound passes. The reader should note that these are the regions where no periodic modulation was observed in the ion and low-energy electron fluxes.

From 40 to 90 R_J outbound, Figure 5.17 shows a linearly increasing lag in the phase of the particle modulation. Such a lag could be the result of finite propagation velocity of the disturbance produced by the rotating tilted dipole [Northrop, Goertz, and Thomsen, 1974]. In deriving a mathematical expression for the disc model that includes the delay, Kivelson et al. [1978] also included the possibility that the disc may bend toward the equator at larger distances. In terms of r, δ, and λ coordinates (radial distance, latitude and System III (1965) longitude), the plasma sheet position is given by:

$$\lambda = 20.8 \mp \cos^{-1} \frac{\tan \delta}{\tan \delta_0} + 36.27 \frac{r - r_0}{v} \tag{5.15}$$

In this expression δ_o is the inclination of the plasma sheet at distance r, the delay "velocity" is represented by v, and, r_o is the distance at which the rigid disc model breaks down.

Figure 5.18 illustrates the evolution of a rigid disc into the bent twisted disc. This is accomplished by twisting the disk through an angle $\theta = 36.27\ (r - r_o)/v$ around the spin axis and then bending it toward the equator. In Figure 5.18*b*, the parameters δ_o, r_o,

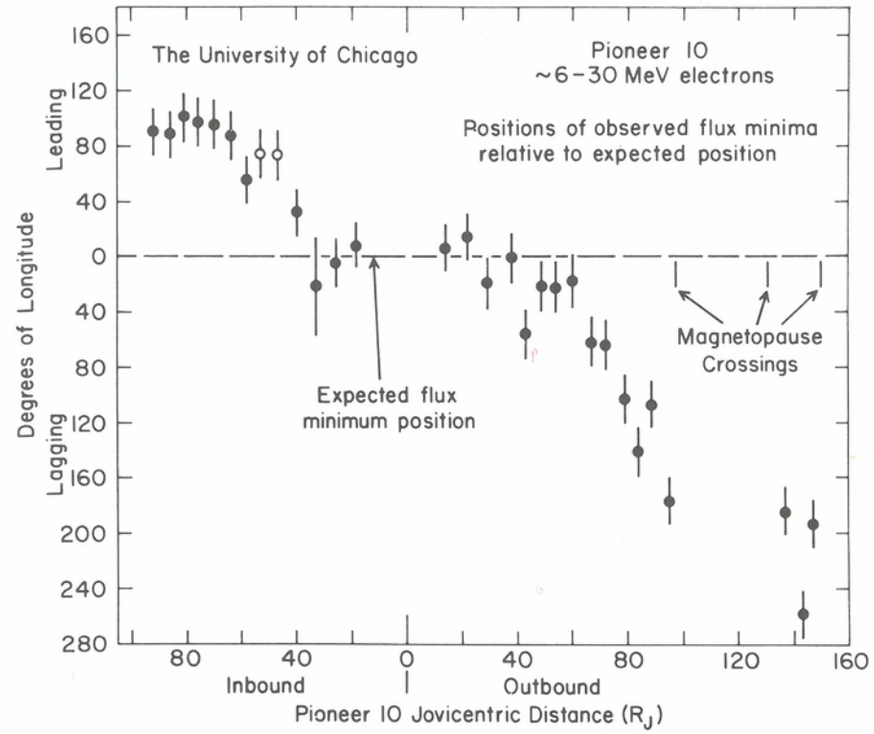

Fig. 5.17. Phase of flux minima of ~6- to 30-MeV electrons relative to the position expected from rigid corotation with the magnetic equator at the dipole equator (rigid disc model). Data were taken by the University of Chicago experiment on Pioneer 10. Solid circles correspond to periods when the spacecraft was in the magnetosphere; open circles indicate a period of possible reentry into the magnetosheath [from McKibben and Simpson, 1974].

and v are independent of solar aspect and of longitude; however, this is not a basic feature of the model. As a matter of fact, we know that solar aspect affects the radial extent of the plasma sheet, and one might expect that δ_o would be smallest in the antisolar direction because the plasma sheet will eventually merge into the neutral sheet of the magnetotail; therefore, Figure 5.18*b* does not illustrate a snapshot of the plasma sheet position but the configuration that appears to rotate past an observer at a specific local time.

The application of this model to Pioneer 10-out data is simple because the latitude of the trajectory was approximately the same as the dipole tilt (9° vs. 10°); thus, only one flux maximum was observed and the $\pm \cos^{-1}(\tan \delta / \tan \delta_o)$ term in Equation 5.15 could be ignored. Little bending towards the equator could have occurred; otherwise, flux maxima (Fig. 5.14) would not have been observed out to the magnetopause. Bending due to the centrifugal stress had been expected [Hill, Dessler, and Michel, 1974; Smith et al., 1974]; however, this will not occur if the plasma temperature is equal to or larger than the corotation energy of a few keV [Goertz, 1976b], and Voyager measurements have confirmed that this is, indeed, the case (Chap. 4). The phase lag (Fig. 5.17) can then be analyzed as a "velocity"; and values from 29 to 43 R_J/hr were obtained, depending on fitting criteria used [Kivelson et al., 1978].

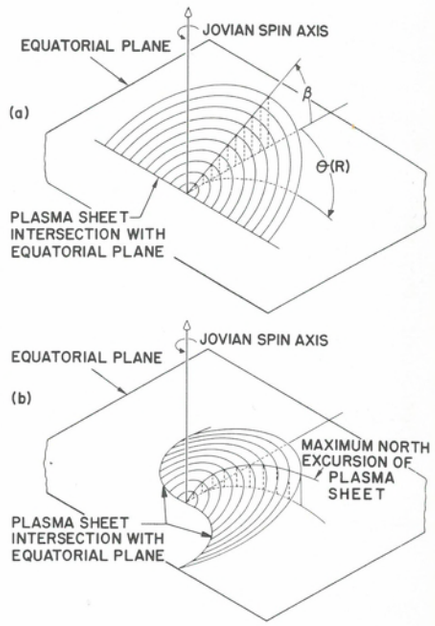

Fig. 5.18. Isomeric projection of the neutral sheet configuration as described by the rigid disc (Fig. 5.18*a*) and by the bent twisted disk (Fig. 5.18*b*). The disc is illustrated by equally spaced concentric circles, and the z dimension has been multiplied by three to enhance the dipole tilt. $\theta(R)$, in Figure 5.18*a* shown in the equatorial plane, is the delay angle used in computing Figure 5.18*b*. In both figures, the inclination of the inner ring is 10.4°, but decreases to 6.4° for the outer ring in Figure 5.18*b* [from Schardt, McDonald, and Trainor, 1981].

For the lower latitude trajectories of Voyagers 1 and 2 outbound, the disc model predicts two crossings per 10 hr as long as $\delta < \delta_o$; and, indeed, two were found consistently out to 70 R_J and frequently beyond that distance (Fig. 5.15). The analysis of these data is more complex because the Voyager trajectory covered the latitude range from $\delta = -1°$ to 5°. The contributions of the $\cos^{-1}$ term in Equation 5.15 becomes significant but has not been taken fully into account in some published work. As can be seen from Figure 5.15, the two peaks move together as the radial distance increases from 20 to 70 R_J. The decrease in longitudinal separation is substantially greater than can be accounted for by the increase in spacecraft latitude if the magnetic equator stays at the dipole equator, $\delta_o \simeq 10°$. This effect can be explained in terms of a gradual bending of the plasma sheet toward the equator, or as a difference in propagation speed at the longitudes of the two crossings. The latter explanation is employed in a model combining features of the disc and magnetic anomaly models and will be discussed later.

If the propagation velocity is independent of longitude, then Equation 5.15 can be solved for δ_o as a function of the difference in longitude, $\Delta\lambda$, of the two crossings:

$$\delta_o = \tan^{-1}(\tan \delta / \cos 1/2\ \Delta\lambda) \tag{5.16}$$

Voyager 1 data show that the bending away from the dipole equator ($\delta_o = 10°$) started between 20 and 30 R_J, and that the local inclination, δ_o, near 140 R_J was about 5° [Bridge et al., 1979b]. The bending during the Voyager 2 mission was somewhat less because double peaks occurred out to 200 R_J (Fig. 5.15). This version of the bent twisted disc organizes the data quite well, as can be seen in Figure 5.19, which shows the phase delay vs. distance after the raw data have been corrected for the $\cos^{-1}(\tan \delta / \tan \delta_o)$ term. The resulting "velocities" between 20 and 55 R_J are about 20 R_J/hr, which is somewhat smaller than observed with Pioneer 10. Beyond 70 R_J, the "velocity" increased into the 50 to 200 R_J/hr range.

One explanation for the difference in δ_o between the Pioneer 10 and Voyager missions invokes a local time effect [Thomsen and Goertz, 1981a; Behannon, Burlaga, and Ness, 1981], which is analagous to the behavior of the neutral sheet in the terrestrial magnetosphere. At the Earth, the full wobble of the magnetic dipole can be seen in the dusk–dawn direction as reflected in the solar-magnetospheric coordinate system [Ness, 1965]. At local times from 1800 to 0600, field lines are pulled back parallel to the plane of the ecliptic and the plasma sheet performs, in essence, a rocking motion about the Sun–Earth line (see Chap. 1 for further discussion). This picture is consistent with $\delta_o \sim 6°$ at 150 R_J for the Voyager 2 trajectory. The Voyager 1 trajectory, however, was closer to dawn (Fig. 5.1*a*) and should have observed a larger, rather than smaller, value of δ_o. The modified disc model would, therefore, require that the full rocking motion of the dusk–dawn plasma sheet does not necessarily propagate throughout the tail. A model for the modulation based on the rocking motion of the Jovian solar-magnetosphere coordinate system [Behannon, Burlaga, and Ness, 1981] is described in Chapter 1.

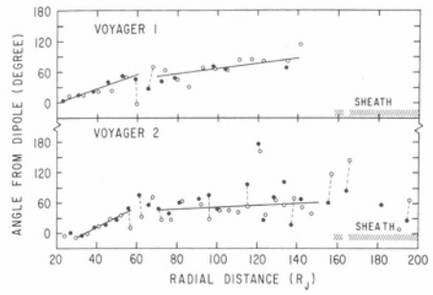

Fig. 5.19. Changes in plasma sheet crossing corrected for lead and lag relative to maximum excursion of bent twisted disc. The angle plotted is $\lambda_{III} - 20.8 \mp \cos^{-1}(\tan \delta / \tan \delta_o)$, where δ is the local spacecraft latitude and δ_o is fit to $\Delta\lambda$ as derived from Equation (5.16). Solid circles refer to crossings or approaches from north to south which occur in the active hemisphere and open circles refer to south to north crossings or approaches [from Schardt, McDonald, and Trainor, 1981].

In the magnetic anomaly model, the plasma density is higher in the active sector and the Alfvén velocity is presumably lower. Thus, the disturbance would propagate more slowly for the north-to-south crossings of Voyagers 1 and 2 than for the south to north crossings. The phase of the modulation can be accounted for on this basis [Schardt, McDonald, and Trainor, 1981] without requiring a bending of the plasma sheet towards the ecliptic (the reader is referred to Vasyliunas and Dessler, 1981, for a further discussion of this model). The major problem with the disc-anomaly model is that the plasma sheet did not cross Voyager 1 beyond 80 R_J [Ness et al., 1979a] as would be required by the 10° tilt. Similarly, Voyager 2 did not cross the sheet consistently beyond 100 R_J. Thus, the disc-anomaly model requires drastic changes of the current sheet topology, and, hence, in current sheet properties beyond about 80 R_J. Such changes are not apparent in the plasma data (Chaps. 3 and 4).

In summary, we can conclude that the strong periodic modulation is caused by the motion of the plasma sheet in response to the disturbance set up by the tilted spinning dipole. The overall modulation of the electrons, protons, and heavier ions is in phase and extends to ~45 R_J in the subsolar hemisphere and within ~20 R_J of the magnetopause in the predawn magnetosphere. Available data are inadequate to specify uniquely the plasma-sheet configuration. The bent, twisted disc model permits an excellent fit to the data [see also Carbary, 1980]; however, the disc-anomaly model (Chap. 10), and in the tail, the rocking plane model (Chap. 1), have not been ruled out. Knowledge of the current sheet motion is required for calculating scale heights in the plasma sheet from the time variation of particle fluxes; and beyond 30 R_J, a thicker plasma sheet is obtained from the anomaly model than from the bent twisted disc model. In the outer magnetosphere and boundary layer of the predawn magnetosphere, electrons show a small 10-hr modulation that apparently does not affect protons or ions. This modulation is also seen in interplanetary electrons of Jovian origin and is discussed in the next section.

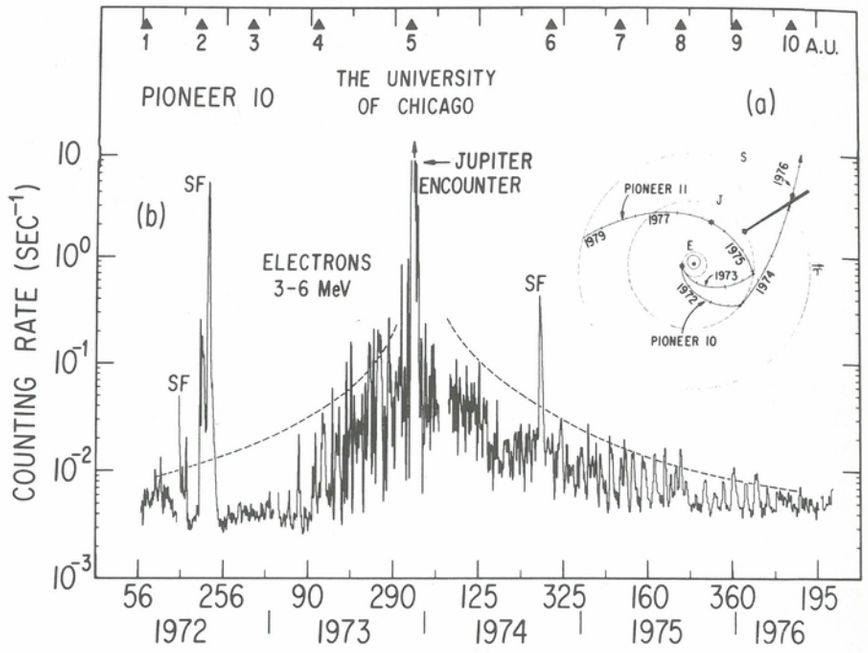

Fig. 5.20. Twenty-four-hour averages of the 3- to 6-MeV electron counting rate observed with the University of Chicago instrument on Pioneer 10. Features identified as SF are of solar flare origin. An intensity dependence of $1/r$ (distance from Jupiter's orbit) is indicated by the dashed line. The solid triangles at the top of the figure refer to Pioneer 10–Sun distances in a.u. The insert shows the Pioneer 10 and 11 trajectories [from Pyle and Simpson, 1977].

5.5. Jovian cosmic rays

Jupiter is an important source of interplanetary electrons in the range 0.2 to 40 MeV. Jupiter also may be a source of interplanetary protons in the MeV range [Simpson et al., 1975]; however, these protons make at most a minor contribution to the ambient flux, and for this reason it has been impossible to establish whether or not protons are emitted. Low-energy ions (<0.5 MeV) of Jovian origin have also been found and resemble the particles observed upstream from the Earth's bow shock (Chap. 4).

The 3- to 6-MeV electron flux in interplanetary space is shown in Figure 5.20. Solar electron events can be identified by their association with solar activity and their softer spectra. The intensity of Jovian electrons falls off as $\sim 1/r$ and is strongly modulated by interplanetary conditions. The regular modulation, especially obvious between 7 and 9 a.u. in Figure 5.20, is due to corotating interaction regions (CIR) that are formed by fast solar wind streams. These regions form an effective barrier and may even influence the release of electrons from Jupiter's magnetosphere. Because electrons move more easily along magnetic field lines than diffuse across them, higher electron fluxes are observed on field lines that connect with the Jovian magnetosphere. For a discussion of interplanetary propagation, the reader is referred to Conlon [1978] and references therein.

The electron spectrum between 0.2 and ~ 10 MeV can be represented as a power law, $E^{-\gamma}$, with $\gamma = 1.5$ [Teegarden et al., 1974]. The spectrum starts to become steeper

above 6 MeV and falls into the range $\gamma = 2.5$ to 4. As a matter of fact, the spectral index is modulated with Jupiter's synodic period, and reaches its maximum ($\gamma = 3$ to 4) when the System III (1965) longitude of 240° is at the subsolar point. This modulation has been detected out to 10^8 km from Jupiter and is associated with an intensity modulation of >6 MeV electrons [Chenett, Conlon, and Simpson, 1974]. The electron modulation was also observed by the Voyager missions and softest spectra still occurred at the same subsolar longitude. Preliminary analysis of the Voyager data demonstrated a clear modulation at distances between 5 and 7×10^7 km from Jupiter and showed that the depth of the modulation is changable [Schardt, McDonald, and Trainor, 1981].

The exact nature of this "clock" modulation of the energetic electron flux in the outer magnetosphere and interplanetary space has not been established. McKibben and Simpson [1974] suggested that the energetic electron flux varies simultaneously throughout the outer magnetosphere, especially near the magnetopause. Clearly, the modulation depends on the aspect of the Jovian magnetic field to the solar wind direction. The magnetic anomaly model [Dessler and Hill, 1975 and 1979] explains the modulation by an increased ionospheric conductivity that is produced by precipitating electrons at a magnetic anomaly between $\lambda_{III} = 200$ and 270°. The increased plasma pressure at these longitudes opens additional field lines when the plasma expands into the tail and thus releases a larger electron flux.

An examination of the time delay associated with the expansion of magnetospheric plasma and the phase of the modulation places the most likely release point along the dawn magnetopause at local times from 0200 to 0800. The most characteristic feature of the "clock" modulation is a sharp decrease in the electron flux ($E > 6$ MeV) that lasts only about two hours during each cycle. Because electron diffusion across the magnetopause is enhanced by plasma loading, this flux minimum should occur at a time when a minimum density of the expanding plasma corotates into the dawn magnetopause. Such a minimum would occur [Schardt, McDonald, and Trainor, 1981] at the boundary between the active and inactive hemispheres, if the combination of expansion and partial corotation leads to a rarefaction region between the two plasma streams. Beyond 20 R_J, the active hemisphere, because of its greater plasma loading, is expected to move at a smaller fraction of the corotation velocity than the inactive hemisphere, thus producing a separation as the two regions expand into the tail and rotate across it (see also Chap. 10 and the discussion of rotational modulation in this chapter).

The source strength of Jupiter as a cosmic-ray electron source can be estimated in several ways. The simplest method uses the total electron flux and its first-order anisotropy near the magnetopause. This gives the local loss rate and one has to assume that the loss rate is the same over an extended surface. A loss rate of $\sim 10^{24}$ electrons s^{-1} above 6 MeV was derived based on data from the Pioneer 10-out pass and a surface area equal to that of a 100 R_J sphere [Fillius, Ip, and Knickerbocker, 1977]. Another method is to estimate the total number of Jovian electrons in the heliosphere and assume that their residence lifetime is the same as the known lifetime of solar electrons. This gives a source strength of 10^{25} to 10^{26} electrons s^{-1} [Fillius, Ip, and Knickerbocker et al., 1977]. Conlon [1978] fitted a diffusion-convection model to the observed distribution of Jovian electrons in the heliosphere and used best estimates of the diffusion coefficients to obtain a differential source strength in the range 0.2 to 10 MeV:

$$j(E) = 1.6 \times 10^{26} E^{-1.5} \text{ MeV}^{-1} \text{ s}^{-1} \tag{5.17}$$

The total power required to produce these electrons can be calculated from the known spectra and estimates of the source strength. For the total flux above 0.2 MeV,

this amounts to 10^{13} to 10^{15} W, based on the estimates by Fillius, Ip, and Knickerbocker [1977] and 2×10^{14} W, based on Conlon's [1978] estimate. It is not obvious where this energy comes from. It is often said that Jupiter's rotational energy is sufficient; however, if this rotational energy is used, one must also find a mechanism for removing angular momentum. Whether the torque that can be exerted on the planet by a magnetosphere–ionosphere–atmosphere coupling is large enough is discussed in Chapter 11.

5.6. Summary and discussion

Processes discovered in the Earth's magnetosphere occur, in general, also at Jupiter. The major exception is the decay of albedo neutrons as a significant source of energetic protons, which is important in the terrestrial magnetosphere. Because of the strong Jovian magnetic field, and hydrogen atmosphere, fewer albedo neutrons are produced. Furthermore, other processes accelerate protons to high enough energies (10–200 MeV) to mask the small contribution from albedo neutrons. In contrast, the adiabatic theory of particle motion [Northrop, 1963] and theories of particle diffusion through the magnetosphere [Schultz and Lanzerotti, 1974] are directly applicable if account is taken of the electric fields due to Jupiter's rapid rotation. Thus, fluxes, energies and first-order anisotropies of energetic ions, protons, and electrons can be interpreted in terms of inward diffusion with the conservation of the first and second adiabatic invariants. In this process, the energy gain is approximately proportional to the increase in field strength; thus, the higher intensity of energetic particles in the inner Jovian magnetosphere is at least in part due to the tenfold higher magnetic field strength. Another result of the high field strength is that Jupiter's inner magnetosphere is well insulated from solar wind fluctuations. It is, therefore, believed that the fluctuations responsible for the particle diffusion are not due to the solar wind but to winds in Jupiter's ionosphere. Another important source of fluctuating electric fields is the centrifugal gradient drift instability at the outer edge of the Io torus (Chap. 3). This instability could cause enhanced diffusive transport in the outer Io torus. As in the radiation belts of the earth, particles are lost into the planet's atmosphere by pitch-angle scattering due to resonant interaction with electromagnetic whistler waves.

A new, not yet completely understood, phenomenon is the absorption of energetic particles by the ring and satellites of Jupiter. The original theories of absorption by moons, based on geometric absorption, are inadequate to explain observations [Thomsen, 1979]. Because of the moon's finite conductivity, a current system is set up in the interaction with the corotating magnetosphere; and it is probably the interaction with this disturbance that is the primary mechanism for particle loss. Near Io, interactions with the plasma torus further complicate the situation.

Given the particle population at the boundary between the inner and middle magnetospheres, the "lossy radial-diffusion model" can explain the intensities and energies of particles in the inner magnetosphere; however, solar-wind particles diffusing into the magnetosphere cannot gain enough energy by this process to supply the observed fluxes at this boundary. Thus, an additional acceleration mechanism must be active in the middle and outer magnetosphere. The first model to specifically address this problem was the recirculation model of Nishida [1976] and Sentman, Van Allen, and Goertz [1975, 1978], in which particles diffuse to large L values at a high latitude and then gain further energy as they diffuse back in the equatorial region. In the middle magnetosphere, the electron population follows, in general, stable trapping theory, and

the angular distribution (dumbbell) for $R \leq 25\ R_J$ conforms to the recirculation model. In contrast, the energetic proton population is affected more strongly by dynamic processes and has a pancake angular distribution in the middle magnetosphere. Therefore, the recirculation process probably plays, at most, a minor role in the energization of ions.

A characteristic feature of the middle magnetosphere is the current sheet or plasma disc encircling the planet. It is presumably a direct consequence of the centrifugal stress on the thermal plasma population (Chap. 11). The motion of the current sheet leads to a modulation of particle intensities with two peaks per rotation observed on the low-latitude Voyager spacecraft and only one peak per rotation observed by the Pioneer spacecraft. The disk merges with the tail in the night-side magnetosphere.

Unlike the terrestrial magnetosphere, the β of the magnetospheric plasma is large in the middle and outer magnetospheres. Consequently, these regions are compressible and their radial extent depends sensitively on solar wind pressure (Chap. 3) and on aspect relative to the solar wind direction. The resulting large asymmetry between the subsolar and antisolar hemispheres forms the basis for magnetic pumping [Goertz, 1978; Chap. 10], which could easily supply the required energization. Magnetic pumping is active also in the middle magnetosphere where a day–night asymmetry also exists. However, neither the recirculation nor the magnetic pumping processes can account for the short time variability of fluxes in the middle and outer magnetosphere ($\sim$1 min. timescale). For an explanation of these, we have to look for instabilities in the magnetically confined high β plasma that fills these regions. As has been found, both in the laboratory and in the geomagnetic tail, some instabilities can rapidly release energy stored in the magnetic field and accelerate some particles well above thermal energies. The plasma waves observed throughout the magnetosphere (Chap. 8) are a great aid for identifying the specific processes involved, although one would expect the most important waves to have frequencies below the threshold of the wave experiments flown as yet.

Unique among the planets investigated so far, Jupiter is a strong source of interplanetary electrons. The energy required to accelerate these electrons can be estimated from the source strength and electron spectra. Based upon the limits on the source strength derived by Fillius, Ip, and Knickerbocker [1977], the required power falls into the range of 10^{13} to 10^{15} W. This covers the 2×10^{14} W based on another estimate [Conlon, 1978]. This power can be compared to the total power in the solar wind of $\sim 2 \times 10^{15}$ W striking Jupiter's magnetosphere (80 R_J radius for magnetosphere); one would expect that only a small fraction of this power is available for accelerating electrons. The other potential source of energy, the Jovian angular momentum, is limited by the maximum torque that can be coupled through the ionosphere. For a discussion of this, we refer the reader to Chapters 10 and 11, where a number of models are described that can yield an adequate amount of power derived from the planetary rotation. However, the unique observable consequences of each model are not well defined.

The 9 hr 55 min. modulation of the Jovian interplanetary electron flux requires an asymmetry in the magnetosphere that rotates with Jupiter. The only cause for such an asymmetry found so far is based on the magnetic field configuration and has given rise to the magnetic anomaly model (Chap. 10). Still, the mechanism by which these electrons are accelerated and released into the outer magnetosphere and interplanetary space is poorly understood.

In summary, to account for the properties of the energetic particle population, magnetospheric models (Chap. 10) have to explain the following points:

1. interaction mechanisms with satellites and Io's torus; these mechanisms must account for the characteristics of the Io absorption features as a function of particle species and energy;
2. acceleration of electrons and protons in the middle and outer magnetospheres, both time averaged and on a timescale of a few minutes;
3. the structure and motion of the plasma disc in the middle magnetosphere;
4. access of ions from the Io torus and interplanetary space into the outer magnetosphere and their subsequent acceleration;
5. the clock modulation of energetic electron fluxes in the outer magnetosphere and in the interplanetary medium; and
6. the mechanism for releasing energetic electrons into interplanetary space and modulating this release with the Jovian rotation period.

Answers to these questions will require a better definition of the properties of the energetic-particle population. Some of this information will emerge from further evaluation of Voyager and Pioneer data; however, new observations with more sophisticated instruments are needed. Crucially important are a greater local-time coverage, a larger time base to distinguish spatial from temporal variations, an extended coverage of lower-energy particles, and an extension of the frequency range of wave measurements.

6

SPECTROPHOTOMETRIC STUDIES OF THE IO TORUS

Robert A. Brown, Carl B. Pilcher, and Darrell F. Strobel

6.1. Introduction

A toroidal volume near Io's orbit is made luminous by multiple optical and ultraviolet line emissions excited by resonant scattering of sunlight and by electron collisions. These emitting atoms and ions have been lost from Io. Table 6.1 summarizes the species and detected transitions as of early 1982. In this chapter we focus on spectrophotometric measurements of these emissions and their physical interpretation. The reader is referred to Pilcher and Strobel [1982] for a more general view of torus emission phenomenology.

The concept of circumplanetary atoms of satellite origin was first proposed by McDonough and Brice [1973] for Titan, a satellite with a dense atmosphere from which Jeans escape is probably important. The Io phenomenon was not anticipated owing to Io's low atmospheric pressure [Smith and Smith, 1972; Pearl et al., 1979]; nevertheless, the discovery by R. A. Brown [1974] of sodium optical emission from Io's vicinity established the first example of a satellite that is a rich, continuing source of material for a planetary environment. We know now that the flow of material from Io dominates the particle and energy budgets of the Jovian magnetosphere.

The primary spatial reference here is to a toroidal volume of $\sim 4 \times 10^{31}$ cm^3 between about 5 and 7 R_J from Jupiter, which includes Io's orbit but lies near the magnetic equatorial plane or centrifugal symmetry surface. This torus contains the bulk of Io's neutral atom clouds and coincides roughly with the UV source region seen by Voyager.

We refer here approximately to the Voyager epoch, the period of the most comprehensive observations. There is intriguing but sometimes conflicting evidence about the plasmasphere's long-term stability, which casts a shadow across the deductions that follow. Spatial inhomogeneity and short-term variability undoubtedly exist. Our simplified picture, based on average properties, is inadequate for such detail and presents some danger of missing a fundamental point associated with, say, nonlinearity or disequilibrium. Nevertheless, we are led by many lines of inference to well-delineated spatial, energetic, and compositional regimes for Jupiter's thermal plasma.

Eight years of study of the manifold emission phenomena associated with the Io torus have produced two kinds of results: (1) demonstrations that certain physical processes obtain in the torus and (2) inferences about the composition and physical state of the torus based on theoretical understanding of the various mechanisms of light production. It is our purpose in this chapter to review these observations, their rationale and implications, plus their relationship to in situ studies of the Jovian environment by the Pioneer and Voyager spacecraft.

6.2. Observational basis: apparent emission rates

This section states the geometrical relationship between the emission and the remote observation of light, incidentally defining the Rayleigh, the photometric unit for